[CANCER RESEARCH 63, 1936–1942, April 15, 2003]

Near-Infrared Fluorescent Imaging of Tumor Apoptosis[1]

Alexander Petrovsky,[2] Eyk Schellenberger,[2] Lee Josephson, Ralph Weissleder, and Alexei Bogdanov, Jr.[3]

Center for Molecular Imaging Research, Massachusetts General Hospital, Charlestown, Massachusetts 02129

ABSTRACT

Noninvasive imaging using radioactive annexin V is an emerging strategy for the assessment of cell death *in vivo* (F. G. Blankenberg, and H. W. Strauss. Apoptosis, *6:* 117–123, 2001.). Therefore, we investigated whether annexin V labeled with the fluorophore Cy5.5 (Cy) could serve as a probe for imaging of tumor apoptosis using near infrared fluorescence (NIRF). We prepared active Cy-annexin (an equimolar dye:protein ratio) that bound to apoptotic Jurkat T cells and an inactive Cy-annexin probe (>2 dyes/mol protein) that did not. Active Cy annexin was used to image a 9L gliosarcoma, constitutively expressing green fluorescent protein marker, and the CR8 variant of Lewis lung carcinoma, stably transfected to express DsRed2. The expression of transfected fluorescent protein provided an indication of tumor margins and a means of defining tumor-associated NIRF signal intensity with both tumor models. Tumors were imaged with and without cyclophosphamide treatment. In both tumor models active Cy-annexin V tumor NIRF signal increased two to three times after the treatment. Tumor NIRF signal developed by 75 min after active Cy-annexin injection and remained for a 20-h observation period. Inactive annexin V was used as a control in the CR8 carcinoma experiments and resulted in a low nonspecific signal. With the 9L gliomosacrcoma model, active Cy-annexin V bound to both tumor cells (Cy-annexin V staining only) and endothelial cells (costained with Cy-annexin V and antibody to the endothelial marker CD31). Our results demonstrate that active Cy-annexin can be used as a NIRF probe to image apoptosis from outside an intact living animal and may provide nonradioactive method of measuring the antiproliferative effects of cancer chemotherapeutic regimens.

INTRODUCTION

Programmed cell death (apoptosis) is fundamentally important for normal development (during embryogenesis and normal tissue homeostasis) and plays an important role in many diseases, including cancer (1). A method of imaging apoptosis in a living organism, particularly one that would allow semiquantitative assessment of apoptosis and, therefore, its progression or regression, could prove valuable in a variety of disease states including tumor chemotherapy and pathologies with an immune component (insulitis, allograft rejection). Imaging apoptosis might involve detecting any one of a large number of markers involved in apoptosis and use imaging modalities ranging from scintigraphy to magnetic resonance imaging (2–7).

One of the earliest markers of apoptosis is the externalization of aminophospholipids that normally reside on the cytoplasmic leaflet of plasma membrane and which are recognized by annexins (8–10). Externalized aminophospholipids (primarily, phosphatidyl serine) are recognized by phagocytes (11) and, possibly, by homotypic neighboring cells (12) as a powerful signal initiating dead cell removal. The presence of apoptotic cells *in vivo* is usually transient, *i.e.*, there is a limited period of time between the onset of apoptosis and the eventual cell removal (13). Therefore, the detection of apoptosis ideally should be accomplished using a high-affinity ligand with a fast rate of clearance from circulation. In this regard, the expression of aminophospholipids on the cell surface enables efficient detection of apoptosis using annexin V, a 36 kDa protein that exhibits a high-affinity calcium-dependent diacyl phosphatidyl serine binding (a K_d in a range of 1.10^{-10} to 7.10^{-9} M-1 has been reported; Refs. 14, 15). Imaging apoptosis through phosphatidyl serine exposure using annexin V is based on the extracellular marker detection, obviating the need for cellular internalization. In addition, the molecular weight of annexin V (36 kDa) permits rapid renal clearance and reduction of background levels of label in the blood.

Techentium-99m-labeled annexin V has been used in conjunction with scintigraphy to visualize cell death *in vivo* (16–18), and is expected to have clinical applications in imaging apoptosis in rejected allografts (19) and evaluating of tumor response to chemotherapy and radiotherapy (20, 21). However, this method is hindered by the relatively low spatial resolution of scintigraphy and the need to use radioactivity. For imaging cell death in tumors, the alternatives to radioactive annexin include superparamagnetic annexin and synaptotagmin conjugates (22, 23), or fluorescent annexin probes. FITC-annexin V is currently in a wide use as a research reagent for apoptosis detection in flow cytometry (24, 25) as well as for *in vivo* microscopy of cardiac cell death (26). Tagging of annexin with a fluorophore results in a probe that is similar to native annexin V in that modification does not significantly alter protein mass, and preserves high affinity and specificity. However, high absorption and scattering of green fluorescence of FITC in tissues would limit its applicability for tumor imaging *in vivo*. We hypothesized that by replacing fluorescein with the near-infrared indocyanine fluorophore (Cy[4]) one could design a probe ("Cy-annexin") detectable in intact live animals. The use of far-red and near-infrared fluorescent reporters (fluorescent in the range of 650–800 nm) has several advantages for *in vivo* imaging: (*a*) high transmittance of tissues and blood to near-infrared light as opposed to the visible light; (*b*) low interference of scattered light used for exciting fluorescence; and (*c*) nonionizing photons serve as the source of fluorescence excitation. Therefore, using near-infrared range of excitation/emission of the spectrum fluorescence signal can be excited in the deeper layers of tissue than in the case of visible light (reviewed in Ref. 27). The experimental proof of the feasibility of NIRF imaging in tumors (wavelength range, 700–850 nm) using fluorescence-mediated tomography has been demonstrated recently (28, 29). Here we report the successful imaging of apoptosis induced in tumors by CPA using as a probe indocyanine-labeled annexin and a NIRF imaging method.

MATERIALS AND METHODS

Purification of Annexin V. Annexin V was obtained from Theseus Imaging Corp. (Cambridge, MA) and was identical to that used clinically (17, 18). Annexin V was concentrated and dialyzed against 0.1 M bicarbonate (pH 8.0) using Centriprep 10 (Millipore, Milford, MA) at 3000 × *g* at 4°C.

Received 8/16/02; accepted 2/19/03.

The costs of publication of this article were defrayed in part by the payment of page charges. This article must therefore be hereby marked *advertisement* in accordance with 18 U.S.C. Section 1734 solely to indicate this fact.

[1] Supported in part by 1P50CA86355-01 (Project 2) and 5RO1 CA74424-01 (to A. B.). E. S. received support from Deutsche Akademie der Naturforscher und Mediziner Leopoldina.

[2] These authors contributed equally to this paper.

[3] To whom requests for reprints should be addressed, at Center for Molecular Imaging Research, Room 5420, Massachusetts General Hospital, Building 149, 13th Street, Charlestown, MA 02129. Phone: (617) 726-5788; Fax: (617) 726-5708.

[4] The abbreviations used are: Cy, Cy5.5; GFP, green fluorescent protein; DsRed2, red fluorescent protein mutant of *Dyscosoma* genus; NIRF, near-infrared fluorescence; Cy-annexin, Cy5.5-annexin V covalent conjugate; CPA, cyclophosphamide; TUNEL, terminal deoxynucleotidyl transferase-mediated nick end labeling; CD31, cell adhesion molecule-1.

Labeling of Annexin V with Cy. To active annexin V [0.3 ml, 3 mg/ml in 0.1 M bicarbonate (pH 8.0)] were added the contents of two vials containing Cy mono hydroxysuccinimide ester (~2 mg; Amersham-Pharmacia, Piscataway, NJ) dissolved in 40 μl of DMSO. The reaction mixture was incubated for 1 h at room temperature. A covalent conjugate of Cy-annexin was separated from nonreacted Cy by double spin separation on columns filled with BioGel P6 (Bio-Rad, Hercules, CA) equilibrated with PBS (pH 7.4). The concentration of coupled Cy dye was determined spectrophotometrically (E_{678} = 250,000 $M^{-1}cm^{-1}$). Protein concentration was determined using BCA Assay (Pierce-Endogen, Rockford, IL). Active Cy-annexin had, on the average, 1.1 Cy molecules bound per mol of annexin. To synthesize inactive Cy-annexin (>2 mol of Cy/mol protein), a 10-times higher ratio of Cy:annexin V was used to achieve a higher degree of amino group modification. Both types of purified labeled annexin V probes were analyzed using SDS electrophoresis. Fluorescence intensity of Cy was measured at λ_{ex} 675 nm/λ_{em} 694 nm. Fluorescence quenching was assessed after treating labeled annexins with trypsin (100 μg/ml, 2 h at 37°C). The radioiodination of Cy-annexin was performed using Iodogen-coated tubes and sodium [^{125}I]iodide as suggested by the manufacturer (Pierce-Endogen). Serum-albumin saturated BioSpin P6 columns (Bio-Rad) were used for [^{125}I]Cy-annexin purification.

Evaluation of Cy-Annexins *in Vitro*. To test the biological affinity of Cy-annexins, apoptosis was induced in Jurkat T-cell lymphoma cells (Clone E6-1; ATCC TIB-152) by treatment with camptothecin (7 μM camptothecin for 5–6 h in complete cell culture medium; 10% FCS, RPMI 1640). After washing, cells were stained using a mixture of propidium iodide and fluorescein-labeled annexin V (ApoAlert; Clontech, Palo Alto, CA) in 1.8 mM $CaCl_2$, 10 mM HEPES, 150 mM NaCl, 5 mM KCl, and 1 mM $MgCl_2$ (pH 7.4). In parallel experiments, cells were incubated with various dilutions of Cy-annexin (both active and inactive preparations). In some experiments, cells were double-labeled with FITC- and Cy-annexins. Cells were analyzed using FACSCalibur (Becton Dickinson, Lexington, KY). The signal difference between nonapoptotic and apoptotic cells was evaluated by the quotient of the medians of the M1 region of nontreated and the M2 region of camptothecin-treated cells.

Stable Transfection of CR-8 Carcinoma Cell Line with DsRed2. The cDNA encoding DsRed2 was excised using *Hind*III and *Not*I endonucleases from commercially available pDsRed2-1 vector (Clontech), and cloned into the eukaryotic expression vector pcDNA3 vector (Invitrogen, Carlsbad, CA). CR8 variant of Lewis lung carcinoma (Ref. 30; a gift of Dr. Timothy Browder, Children's Hospital, Harvard Medical School, Boston, MA) were grown in DMEM (Cellgro, Mediatech, Washington, DC) supplemented with 10% fetal bovine serum and antibiotics. Cells were transfected at 50–60% confluence using Maxfect (Molecular Research, Herndon, VA) using a DNA complex prepared at the ratio of 1 μg DNA:3 μg Maxfect reagent. Twenty-four or 72 h after transfection, the cells were trypsinized and sorted (FACSVantage; Beckton-Dickinson).

Cell Culture. Stably transfected rat gliosarcoma 9L-GFP-34-1 (31) and CR-DsRed2 line were propagated in 10% FCS and DMEM supplemented with 1 mg/ml G418 (Invitrogen-Life Technologies, Inc., Grand Island, NY).

Animal Models. The procedures below were approved by the Massachusetts General Hospital Animal Care and Use Committee. GFP-expressing tumors were grown in female *nu/nu* mice (Massachusetts General Hospital Radiation Oncology breeding facilities; n = 12; a total of four independent experiments) as described (32). Briefly, 2×10^5 cells in 25 μl of serum-free cell culture medium were injected s.c. into posterior aspect of the ear pinna in anesthetized animals. Animals were used in experiments on days 10–14 after the inoculation, when tumors were 3–4 mm in diameter.

DsRed2 expressing CR8 Lewis-lung carcinoma cells (1.10^5 cells/injection) were injected s.c. bilaterally in mammary fat pad in female *nu/nu* mice (three groups; n = 4 animals/group). Animals were used in experiments on days 7–10 after the inoculation of cells.

Before optical imaging, Cy-annexin V conjugate was injected i.v. via tail vein at the dose of 75 μg annexin V/animal, *i.e.*, 3.1 mg annexinV-Cy/kg. The dose of injected Cy-annexinV was empirically determined as the amount needed to produce a NIRF signal in nontreated animals that would be statistically different from the background signal (approximately two times higher) in the same tissue of the animal before the injection of annexin. CPA (Mead Johnson, Princeton, NJ) was given as a single i.p. injection at 170 mg/kg (33). Animals were subjected to NIRF imaging at 24 h after chemotherapy administration.

NIRF Imaging. Optical reflectance NIRF imaging was performed using a system described previously (34). The light-tight box has been equipped with a 150-W halogen lamp and an excitation filter sets suitable for GFP, DsRed2, and Cy excitation (Omega Optical, Brattleboro, VT). Excitation light homogeneously distributed over the field of view using light diffusers. Anesthetized animals (ketamine/xylazine at 80/12 mg/kg i.p.) were positioned on the glass platen using a template enabling reproducible imaging of animals at the fixed distance from the excitation source. The animals were imaged with tumors facing the glass platen surface. Fluorescence was excited from the skin surface (reflectance mode), and obtained fluorescent images were collected using a 12-bit monochrome CCD (Kodak, Rochester, NY) equipped with a f/1.2 12.5–75-mm zoom lens and emission filters (Omega Optical). Optical images in anesthetized animals were acquired in the following sequence: (*a*) visible light image (to outline the animal); (*b*) fluorescent imaging of the tumor marker (GFP or DsRed2); (*c*) fluorescent image in the NIRF channel before Cy-annexin V injection, to obtain background reflectance image; and (*d*) fluorescent image in the NIRF channel at various times after Cy-annexin injection. A single imaging session required in total ~5 min. Images were digitally acquired as TIFF files and processed using commercially available software (IP Lab Spectrum; Signal Analytics, Vienna, VA). Image processing included segmentation of the fluorescent protein marker images to obtain the outline of the tumor and pasting the segment layer over the near-infrared images followed by the measurement of the fluorescence signal within the borders of the segment. Signal intensities were expressed as average pixel values. The measured signals were normalized using standard solutions of Cy. Fluorescence signal change was determined by subtracting background (preinjection) signal. Statistical significance was analyzed using unpaired t test with Welch's correction.

Histology. Tumors excised from euthanized animals were snap frozen, and cut into 8-μm sections. Some animals were preinjected i.v. with a Cy3-labeled anti-CD31 antibodies (rat antimouse monoclonal, MEC13.3; BD PharMingen) at 20 μg antibody/animal ~15 min before sacrificing to reveal tumor blood vessels. DNA fragmentation in apoptotic cells was assessed in frozen sections using a TUNEL method (ApopTag; Intergen, Purchase, NY). Digoxigenin-labeled dUTP has been revealed using FITC- or Cy3-labeled antidigoxigenin

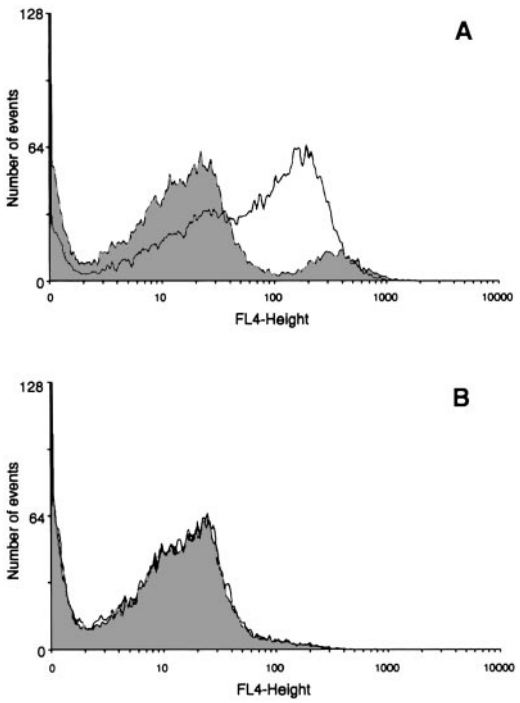

Fig. 1. *A*, flow cytometry of control (*shaded profiles*) and camptothecin-treated Jurkat cells stained with Cy-labeled annexin V (active, equimolar Cy:annexin V ratio). *B*, flow cytometry of Jurkat cells stained using inactive Cy-labeled annexin V (Cy:annexin molar ratio >2).

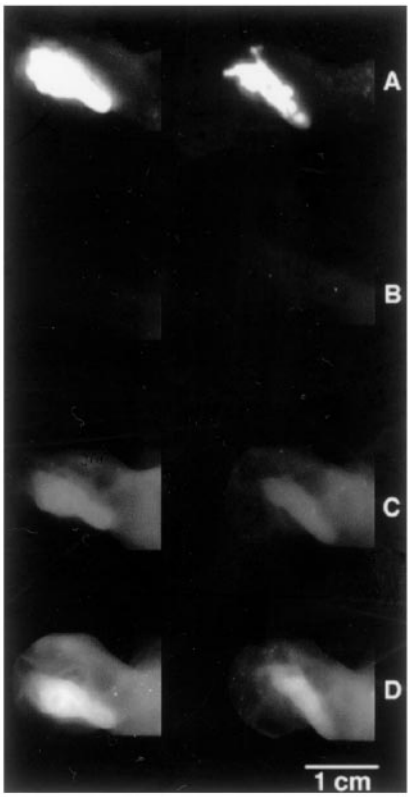

Fig. 2. Imaging of apoptosis in 9L-GFP tumor model implanted in ear pinna (results shown were obtained in two animals in two independent experiments). *A*, expression of GFP, green fluorescent channel; *B*, near-infrared background signal tumors; *C*, active Cy-annexin signal (near-infrared) in tumors before treatment with CPA; *D*, active Cy-annexin signal (near-infrared) in tumors after the treatment with CPA. Animals received an i.p. injection of 170 mg/kg CPA before the reinjection of active Cy-annexin. Imaging was performed as described in "Materials and Methods."

$F(ab')_2$ fragment (Roche Diagnostics, Indianapolis, IN). For quantitation of TUNEL-positive cells, four nonoverlapping fields of view (area, 0.4 mm^2) were analyzed per each tumor tissue section. Three to four nonconsecutive sections were analyzed per tumor sample. Fluorescence microscopy has been performed using an inverted microscope (Zeiss Axiovert 100 TV, Wetzlar, Germany) fitted with appropriate filter sets (Omega Optical). Images were acquired using a Photometrics CH250 CCD (Photometrics, Tucson, AZ), with image acquisition, pseudo-color image fusion, and storage controlled by IP LabSpectrum software (Signal Analytics).

RESULTS

Synthesis of Cy-Annexins and Evaluation *in Vitro*. Recombinant annexin V isolated from *Escherichia coli* was >97% pure by SDS-electrophoresis. Modification of annexin V with the *N*-hydroxysuccinimide ester of Cy at two different ratios of Cy:annexin V (2 mg/mg and 20 mg/mg) resulted in an active annexin V (approximately equimolar Cy:annexin ratio) and an inactive annexin V (>2 residues Cy:annexin molecule), which evaluated for activity as described below. NIRF signal in the gel colocalized with the Coomassie staining at 36–38 kDa protein band using marker proteins (data not shown). Trypsin treatments did not reveal any differences between active and inactive annexins in the degree of indocyanine dye quenching after covalent coupling to annexin.

The ability of annexin V to differentiate between apoptotic and normal cells was assessed using flow cytometry of camptothecin-treated (apoptotic) Jurkat T cells. Using the red diode laser (635 nm excitation) and >670 nm bandpass filter (FL4 channel) cell-associated Cy-annexin was quantified. Cytometry of camptothecin-treated and untreated cells incubated using active annexin V (Fig. 1*A*) showed two distinct populations of active annexin V-stained cells, with the proportion of apoptotic cells increasing because of camptothecin treatment. As expected, camptothecin treatment induced apoptosis and increased the proportion of highly stained cells. Apoptotic cells had a NIRF that was 7–10 times higher than live cells (Fig. 1*A*, *unshaded*). Inactive annexin V (Fig. 1*B*) was unable to distinguish apoptotic from live cells as evident by a single peak of weakly stained cells with or without camptothecin treatment. Additional double label flow cytometry experiments using FITC-annexin V and active Cy-annexin indicated that both annexins reacted with the same cell population present in the cell culture.

9L-GFP Gliosarcoma Tumor Model. The 9L-GFP gliosarcoma tumor was grown in the ear pinna of nude mice and exhibited a bright signal when the fluorescence of GFP marker was visualized. GFP fluorescence provided an outline of the tumors (Fig. 2*A*) to allow the NIRF signal after injection of active Cy-annexin to be clearly defined as emanating from tumor or nontumor tissue (Fig. 2, *C* and *D*). Before injection of active Cy-annexin, tumor signal was low, and the average pixel intensity was not statistically different from that of the surrounding tissue, *i.e.*, no fluorescence from GFP was detectable in the NIRF channel. After animals were injected with active Cy-annexin, a weak NIRF signal at 90 min after injection was obtained from the tumors and from surrounding nontumor tissue (Fig. 2*C*). Animals were then treated with CPA, injected with active Cy-annexin after a 24-h waiting period, and imaged as above. In contrast to nontreated animals (Fig. 2*C*), CPA-treated animals showed a pronounced enhancement of the NIRF signal from the tumor at 75 min after the injection (Fig. 2*D*). The observed NIRF signal increase was measured, corrected for background (preinjection) fluorescence in tumors, and the time course of NIRF tumor signal intensity was obtained (Fig. 3). Tumor NIRF increased to 75 min after injection and was approximately 2–3-fold higher for CPA-treated than non-CPA-treated tumors ($P < 0.05$). A small but significant decrease of tumor fluorescence ($P < 0.05$) was

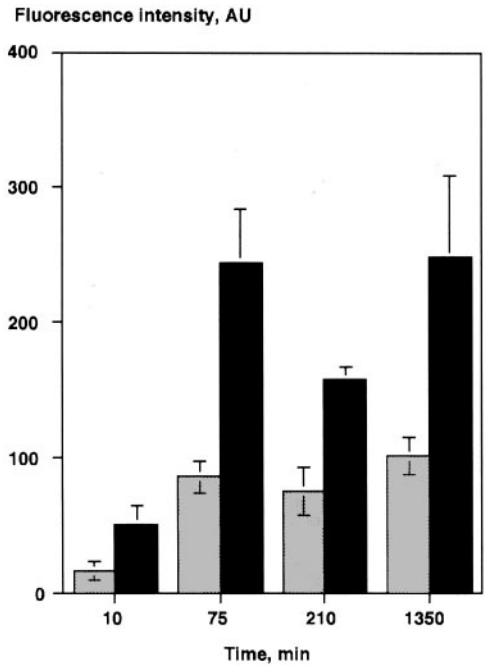

Fig. 3. Time-dependence of NIRF signal intensity measurements in 9L-GFP model. *Shaded bars*, control, nontreated animals ($n = 6$); *solid bars*, CPA-treated animals ($n = 6$). Near-infrared signal measured by placing region-of-interest defined by the area positive for GFP-expression (see Fig. 2). Signal intensity is expressed as median signal with the background fluorescence subtracted. Results are presented as mean; *bars*, ±SD.

observed at later time points followed by an insignificant second increase of the signal at 22 h after the injection (Fig. 3).

To evaluate the frequency and type of cells responsible for the NIRF signal, we performed histology on non-CPA-treated (Fig. 4*A*) and CPA-treated tumors (Fig. 4*B*) after injection of fluorescent-labeled antibodies against mouse platelet-endothelial CD31. As expected, GFP expressing (green) 9L gliosarcoma cells were found throughout the tumor and were the major cell type. Analysis of multiple sections showed the density of cells stained with active Cy-annexin was only 1–2 cells/mm^2 for non-CPA-treated tumors (for example, see Fig. 4*A*) but increased to 17 $\pm$ 4 cells/mm^2 after CPA treatment (Fig. 4*B*). Of interest was the fact that active Cy-annexin binding cells (Fig. 4*B, red*) were only a very small fraction of total cells present for both non-CPA- and CPA-treated tumors. Anti-CD31 stained areas corresponding to vessel-lining endothelial cells (Fig. 4*B, blue*) were less prominent in CPA-treated tumors (compare Fig. 4, *A* and *B*). Infrequent, active Cy-annexin stained cells (Fig. 4*B, red*) could be identified as being endothelial cells (Fig. 4*B, arrowheads*) or 9L gliosarcoma (Fig. 4*B, green*). The low level of Cy-annexin binding to control 9L gliosarcoma tumors correlated with a very low density of TUNEL-positive cells (4 $\pm$ 2 cells/mm^2) in these tumors before CPA treatment.

Ds Red2 CR 8 Lewis Lung Carcinoma Tumor Model. The second *in vivo* cancer model used in the study used a CPA-resistant variant of Lewis lung carcinoma (CR8; Ref. 30). TUNEL analysis performed on histology sections of this tumor obtained from non-treated animals showed a very low incidence of apoptotic cells (8 $\pm$ 3 cells/mm^2) and a very high density of tumor blood vessels (anti-CD31 staining; Fig. 5, *inset*). Upon transfection with GFP, CR8 cells showed a very rapid loss of this marker and proliferation of nonfluorescent cells. Therefore, we obtained a transfectant of CR8 expressing red fluorescent protein DsRed2 (to obtain tumor outlines using optical imaging) and imaged the extent of tumor cell apoptosis after treating the tumor with CPA. All of the tumors showed detectable but variable levels of DsRed2 expression (Fig. 5 and Fig. 6*B*). Necrotic regions of the tumors usually contained very low DsRed2 fluorescence. Red fluorescent protein expression was in most cases useful for outlining the tumor and the correct positioning of region-of-interest in near-infrared images for measuring Cy-annexin-mediated signal in tumors.

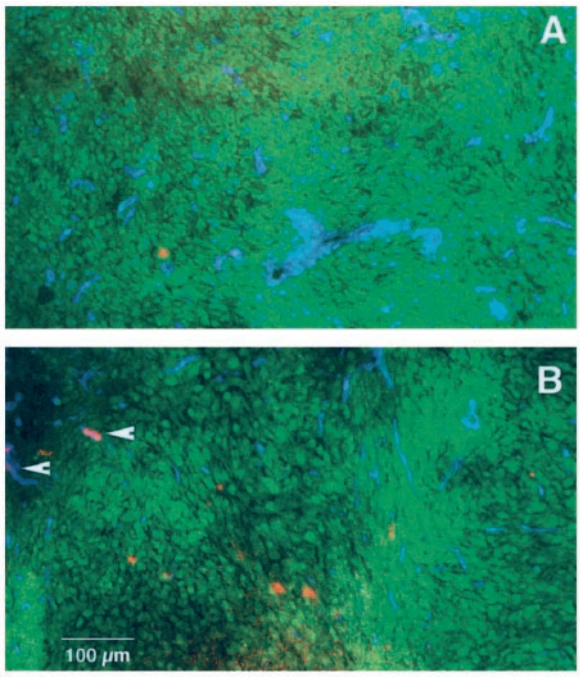

Fig. 4. Histology of 9L-GFP tumor before (*A*) and after (*B*) CPA treatment. Fusion images were obtained by overlaying three pseudo-color images obtained in green fluorescence channel (GFP, coded with *green*); red fluorescence channel (Cy3-labeled anti-CD31 antibodies, coded with *blue*); and far-red fluorescent channel (active Cy-labeled annexin, coded with *red*). *Arrowheads* point to cells costained with anti-CD31 antibodies and annexin demonstrating endothelial cell death.

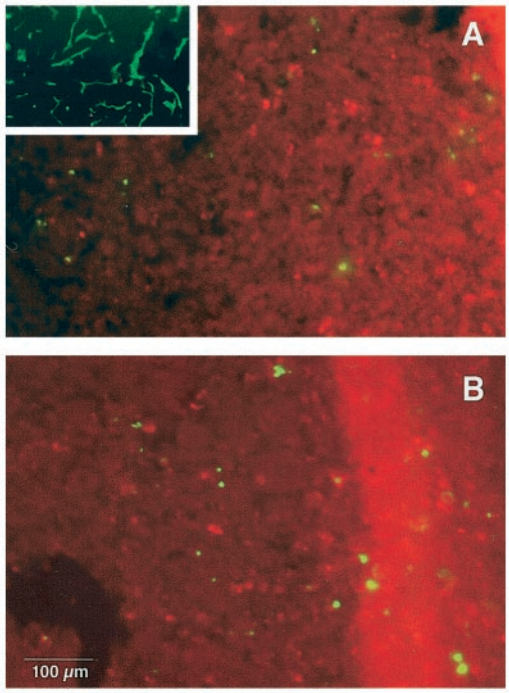

Fig. 5. Histology of CR DsRed2-expressing tumors before (*A*) and after (*B*) CPA treatment. The fusion images were obtained by fusing two pseudo-color images taken in red fluorescence channel (DsRed2, coded with *red*) and green fluorescent channel (TUNEL staining of apoptosis using fluorescein-labeled antidigoxigenin antibodies, coded with *green*). *Inset* (*A*) shows vascular density in nontreated tumors, vascular endothelial cells detected using fluorescent anti-CD31 antibody.

Near-infrared fluorescent tumor images obtained in control animals (nontreated with CPA) showed that there is a measurable low level of active Cy-annexin accumulation in the tumor (Fig. 6). After CPA treatment, fluorescent annexin signal in tumors increased dramatically 75 min after the injection, and the fluorescence of treated tumors remained high for several hours (Figs. 6 and 7). If instead of active Cy-annexin, CPA-treated animals were injected with an inactive Cy-annexin (with a molar ratio Cy:annexin >2), only very low signal in the tissue was observed (Fig. 6). The signal observed after the injection of the inactive annexin was four to five times lower than that of obtained using the active annexin ($P < 0.01$). The difference in measured signal was observed in treated animal group at various times after the injection (Fig. 7). Moreover, the inactive annexin showed a significantly lower ($P < 0.05$) near-infrared signal in tumors of CPA-treated animals than the signal measured in nontreated control animals that received an injection of active Cy-labeled annexin. Tumors obtained from animals that were treated with CPA and subsequently received active or inactive labeled annexins (Fig. 5) showed similar levels of cell death as determined using TUNEL (apoptotic cells are shown in green). The density of apoptotic cells in histology sections was 48 $\pm$ 6 cells/mm^2 in animals that received inactive Cy-annexin and 46 $\pm$ 8 cells/mm^2 in animals injected with active Cy-annexin. To verify the results obtained using NIRF, we coinjected CR8-bearing animals with radioiodinated Cy-annexin V. The results of a biodistribution study performed 90 min after the injection showed that radiolabeled tracer was bound to tumors in treated animals at

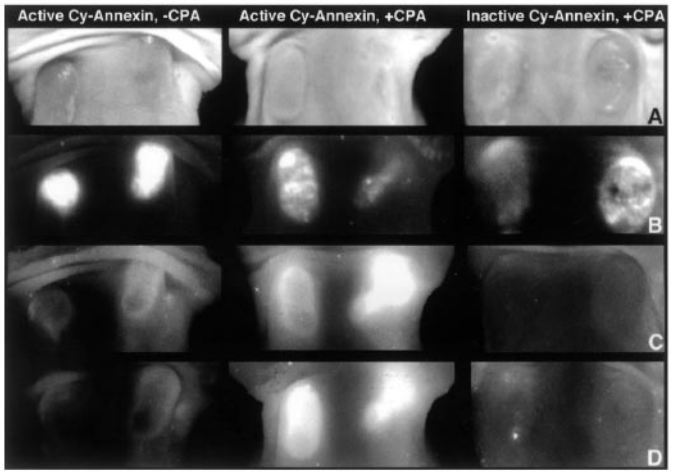

Fig. 6. Imaging of apoptosis in CR-red fluorescent tumor model implanted in mammary pad. Animals were divided into three groups: (*a*) injected with active Cy-annexin and not treated with CPA; (*b*) injected with active Cy-annexin and treated with CPA; and (*c*) injected with inactive Cy-annexin and treated with CPA. *A*, visible light image of implanted tumors; *B*, expression of DsRed2 in CR tumor (red fluorescence channel); *C*, near-infrared signal measured in tumors at 75 min after the injection of Cy-annexin; *D*, near-infrared signal measured in tumors at 20 h after the injection of Cy-annexin. Animals received an i.p. injection of 170 mg/kg CPA. Imaging was performed as described in "Materials and Methods."

12.8 ± 4.9% of the injected dose/g of tissue, whereas control tumors accumulated 4.4 ± 1.6% of the injected dose/g of tissue. The observed difference was statistically significant ($P < 0.05$). The binding of radioiodinated Cy-annexin to the kidney (one of the major sites of annexin accumulation) was similar in both treated (6.9 ± 2.6 injected dose/g) and control groups (8.5 ± 2.4 injected dose/g; $P > 0.05$).

DISCUSSION

Antiproliferative and cytotoxic drugs (chemotherapy), and high-energy photons (radiotherapy) are in wide clinical use for cancer treatment. Noninvasive imaging of cell death in tumors *in vivo* would create means of accurate assessment of the tumor response to a wide variety of antiproliferative treatments. It has been demonstrated that annexin V, a calcium-binding protein with high affinity to the externalized phosphatidyl serine on apoptotic cell plasma membrane, can be used for this purpose. Radioactive ^{99m}Tc-labeled annexin V, which is currently undergoing clinical evaluation (19), can be used for imaging of apoptosis *in vivo* and has been tested extensively in animal models (35–37). Here we demonstrate that an alternative imaging technique (near-infrared fluorescent imaging) can be used for detecting annexin V binding to tumor cells affected by chemotherapy. By covalent modification of annexin with near-infrared indocyanine fluorescent dye (Cy) we obtained two probes that had very similar optical properties and molecular mass, but differed greatly in their ability to interact with apoptotic cells. An equimolar coupling of indocyanine to annexin yielded a probe that was active in standard *in vitro* tests, whereas the additional coupling of indocyanines to the same protein molecule resulted in a probe that behaved as completely inactive *in vitro* (Fig. 1). One potential explanation for this phenomenon is in clustering of lysine residues of annexin V molecule residing in a close proximity to Ca-phosphatidylserine binding centers. It is possible that the overmodification of these lysines with large fluorophores may lead to a loss of affinity to phosphatidylserine (38). We took advantage of this unusual property of annexin to obtain active as well as to control inactive apoptosis probes for *in vivo* imaging experiments in two cancer models.

One of the model tumors, 9L gliosarcoma, stably expresses high levels of GFP marker (9L-GFP) *in vivo* with no apparent cytotoxicity. This model was initially used for testing active Cy-annexin. As demonstrated before, the expression of GFP marker can be extremely useful for *in vivo* experiments for differentiating between the host cells and tumor cells in the case of constitutive (39, 40) or inducible (41) expression of fluorescent protein marker. In our experiments, the expression of GFP (or, alternatively, red fluorescent protein DsRed2) assisted in precise localization of tumors *in vivo*, which was very useful for improving accuracy of quantitation of the tumor-associated near-infrared fluorescent signal measured in a second optical channel. Fluorescent protein marker signal defined the shape of the region of interest, which was used for measuring fluorescence intensity of tumor images obtained in semiquantitative, reflectance mode. The use of tumor-expressed fluorescent marker also enabled a more accurate imaging analysis, including a correction for the background tumor signal (Fig. 2). We found that tumors of animals that received an injection of CPA followed by the injection of active Cy-annexin developed a bright near-infrared fluorescent signal that was absent in the same animals before the treatment (Fig. 2). The signal difference was measurable as early as 10 min after the administration. It should be noted that in the 9L model the background levels of cell death were very low by TUNEL assay, which assisted in detecting CPA-induced cell death in these tumors. Importantly, histology correlation data (Fig. 4) suggests that a substantial number of apoptotic cells in these tumors are endothelial cells of tumor blood vessels, as demonstrated by costaining of annexin V-positive cells with fluorescent anti-CD31 (anti-PECAM-1) antibodies. This finding supports earlier reports documenting CPA-induced antiangiogenesis in tumors (30, 42). Interestingly, after a peak of Cy-annexin-induced fluorescence we observed a significant decrease of Cy-fluorescence in treated 9L-GFP tumors as the initially high fluorescence observed after a single injection of annexin V (at approximately 1–1.25 h after the injection) has been thereafter decreasing. This reproducible effect could be associated

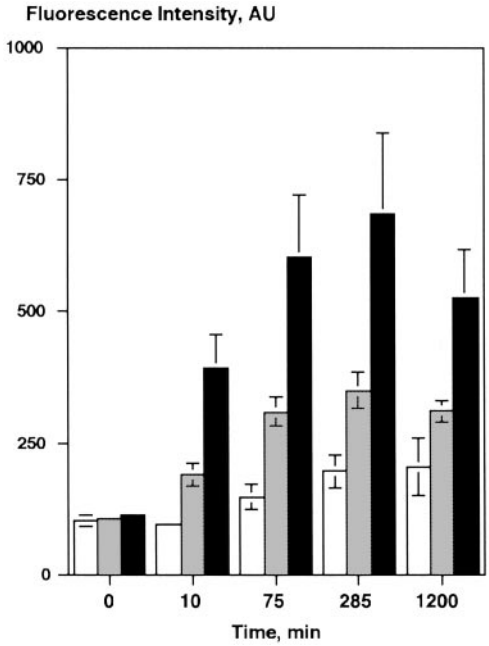

Fig. 7. Time dependence of NIRF signal intensity measurements in CR tumors expressing DsRed2 marker protein. □, control-treated animals injected with the inactive Cy-annexin ($n = 3$); ▨, control animals injected with the active Cy-annexin and left untreated ($n = 6$). ■, animals injected with the active Cy-annexin after treatments with CPA ($n = 6$). Near-infrared signal measured by placing region-of-interest defined by the area positive for DsRed2 expression. Signal intensity is expressed as median signal with the background fluorescence subtracted. Results are presented as mean; *bars*, ±SD.

with the "shedding" of annexin V from the surface of "uncommitted" cells that revert to normal, nonapoptotic phenotype with asymmetric membrane lipids (43) followed by the reappearance of more apoptotic cells in the tumors at the later stage. Alternatively, this effect may be attributed to the removal of the early population apoptotic cells by phagocytes. It is presently unclear whether this phenomenon can be observed in other types of cancer models and deserves additional investigation.

The testing of active *versus* inactive Cy-annexin probes has been accomplished in a different s.c. model (CR8, a variant of Lewis lung carcinoma). These tumor cells were stably transfected with red fluorescent protein because of: (*a*) better stability of expression and lower cytotoxicity of DsRed2 for this particular cell line; and (*b*) better detectability of CR8 tumors in deeper layers of tissue, because red fluorescent light has the ability to travel at longer distances in opaque tissues without being scattered. The latter factor was important, as GFP-expressing Lewis lung carcinomas were undetectable in our experimental setting because of the fact that carcinomas were grown in deeper tissue and because of the insufficient output of the fluorescence excitation source. The level of cell death induced by CPA in CR8 tumors and detected by active Cy-annexin conjugate was strikingly different from the background levels of cell death (Fig. 6), and was not a result of a nonspecific accumulation in treated tumors as demonstrated using the inactive Cy-annexin. The latter probe, fully fluorescent *in vitro*, showed no change of signal in tumors before and after the treatment with CPA. Using the properties of Cy-annexin conjugates described above, we also demonstrated that this effect was not a consequence of variability of cell death levels in individual animals, because we observed approximately the same occurrence of apoptotic cells in tumors of all of the CPA-treated animals (Fig. 5). Two results obtained using the CR8 model suggest that NIRF signal reflects the preference of annexin V for tumors in treated animals and that Cy-annexin binding in tumors correlates with the apoptosis. First, TUNEL analysis of treated and control tumors showed that the number of chemotherapy-induced cell death (48 ± 6 cells/mm^2) was significantly higher than the number of spontaneous cell death in control tumors (8 ± 3 cells/mm^2; $P < 0.05$). Second, the biodistribution performed at the time point corresponding to three half-lives of radiolabeled Cy-annexin (14) showed a 2.5–3 times higher accumulation of the probe in treated CR8 tumors. Interestingly, the time course of near-infrared tumor fluorescence in CR8 tumors fluctuated less than in the 9L model, presumably because of a higher number of CPA-induced apoptotic endothelial cells in these densely vascularized tumors (30) and the overall larger tumor area used for measurements in this study.

In conclusion, we demonstrated that the modulation of cell death induced by CPA can be assessed *in vivo* using a noninvasive optical imaging approach. This nonradioactive method of detection can be highly useful for *in vivo* studies, because the imaging probe does not require labeling every time for the experiment to be performed. Moreover, images can be acquired repeatedly in the same animal, and the results can be scaled to the signal obtained with inactive probe. The active Cy-annexin probe tracks apoptotic cells in tumors and provides a NIRF signal that can be used in semiquantitative assessment of apoptosis levels. The basis for this conclusion is: (*a*) the fact that inactive Cy-annexin resulted in a tumor fluorescence that was similar to background (Fig. 6); (*b*) NIRF signal was associated with a small number of cells in a tumor, as would be expected if the probe binds to cells that undergo apoptosis (Fig. 4); and (*c*) CPA treatment resulted in an overall increase of tumor NIRF signal (Figs. 3 and 7). Although the current study imaged the active Cy-annexin as a NIRF signal from peripheral ectopic tumors, it is feasible to image NIRF from tumors lying deep within small or even large animals (44). Additional advances in instrumentation may permit NIRF imaging of tumor apoptosis with a Cy-annexin to overcome the limitations of surface weighting used here and may allow imaging of apoptosis in a variety of important clinical settings.

ACKNOWLEDGMENTS

We thank Dr. Timothy Browder (Children's Hospital, Harvard Medical School, Boston, MA) for the gift of cyclophosphamide resistant Lewis Lung carcinoma variant. We acknowledge the input of Dr. Maria Simonova in designing the DsRed2-expressing vector, Dr. Nikolai Sergeyev in transfecting and maintaining CR-DsRed2 culture, and Doug Olson (Partners AIDS Research Center) for the help in cell sorting.

REFERENCES

1. Kerr, J. F., Wyllie, A. H., and Currie, A. R. Apoptosis: a basic biological phenomenon with wide-ranging implications in tissue kinetics. Br. J. Cancer, *26:* 239–257, 1972.
2. Chinnaiyan, A. M., Prasad, U., Shankar, S., Hamstra, D. A., Shanaiah, M., Chenevert, T. L., Ross, B. D., and Rehemtulla, A. Combined effect of tumor necrosis factor-related apoptosis-inducing ligand and ionizing radiation in breast cancer therapy. Proc. Natl. Acad. Sci. USA, *97:* 1754–1759, 2000.
3. Blankenberg, F. G., Storrs, R. W., Naumovski, L., Goralski, T., and Spielman, D. Detection of apoptotic cell death by proton nuclear magnetic resonance spectroscopy. Blood, *87:* 1951–1956, 1996.
4. Blankenberg, F. G., Katsikis, P. D., Storrs, R. W., Beaulieu, C., Spielman, D., Chen, J. Y., Naumovski, L., and Tait, J. F. Quantitative analysis of apoptotic cell death using proton nuclear magnetic resonance spectroscopy. Blood, *89:* 3778–3786, 1997.
5. Aboagye, E. O., Bhujwalla, Z. M., Shungu, D. C., and Glickson, J. D. Detection of tumor response to chemotherapy by 1H nuclear magnetic resonance spectroscopy: effect of 5-fluorouracil on lactate levels in radiation-induced fibrosarcoma 1 tumors. Cancer Res., *58:* 1063–1067, 1998.
6. Kline, R. P., Wu, E. X., Petrylak, D. P., Szabolcs, M., Alderson, P. O., Weisfeldt, M. L., Cannon, P., and Katz, J. Rapid *in vivo* monitoring of chemotherapeutic response using weighted sodium magnetic resonance imaging. Clin. Cancer Res., *6:* 2146–2156, 2000.
7. Evelhoch, J. L., Gillies, R. J., Karczmar, G. S., Koutcher, J. A., Maxwell, R. J., Nalcioglu, O., Raghunand, N., Ronen, S. M., Ross, B. D., and Swartz, H. M. Applications of magnetic resonance in model systems: cancer therapeutics. Neoplasia, *2:* 152–165, 2000.
8. Fadok, V. A., Voelker, D. R., Campbell, P. A., Cohen, J. J., Bratton, D. L., and Henson, P. M. Exposure of phosphatidylserine on the surface of apoptotic lymphocytes triggers specific recognition and removal by macrophages. J. Immunol., *148:* 2207–2216, 1992.
9. VerHoven, B., Schlegel, R. A., and Williamson, P. Mechanisms of phosphatidylserine exposure, a phagocyte recognition signal, on apoptotic T lymphocytes. J. Exp. Med., *182:* 1597–1601, 1995.
10. Martin, S. J., Reutelingsperger, C. P., McGahon, A. J., Rader, J. A., van Schie, R. C., LaFace, D. M., and Green, D. R. Early redistribution of plasma membrane phosphatidylserine is a general feature of apoptosis regardless of the initiating stimulus: inhibition by overexpression of Bcl-2 and Abl. J. Exp. Med., *182:* 1545–1556, 1995.
11. Fadok, V. A., de Cathelineau, A., Daleke, D. L., Henson, P. M., and Bratton, D. L. Loss of phospholipid asymmetry and surface exposure of phosphatidylserine is required for phagocytosis of apoptotic cells by macrophages and fibroblasts. J. Biol. Chem., *276:* 1071–1077, 2001.
12. Wiegand, U. K., Corbach, S., Prescott, A. R., Savill, J., and Spruce, B. A. The trigger to cell death determines the efficiency with which dying cells are cleared by neighbours. Cell Death Differentiation, *8:* 734–746, 2001.
13. Fadok, V. A., and Henson, P. M. Apoptosis: getting rid of the bodies. Curr. Biol., *8:* R693–695, 1998.
14. Blankenberg, F., Narula, J., and Strauss, H. W. *In vivo* detection of apoptotic cell death: a necessary measurement for evaluating therapy for myocarditis, ischemia, and heart failure. J. Nucl. Cardiol., *6:* 531–539, 1999.
15. Ravanat, C., Archipoff, G., Beretz, A., Freund, G., Cazenave, J. P., and Freyssinet, J. M. Use of annexin-V to demonstrate the role of phosphatidylserine exposure in the maintenance of haemostatic balance by endothelial cells. Biochem. J., *282:* 7–13, 1992.
16. Tait, J. F., Brown, D. S., Gibson, D. F., Blankenberg, F. G., and Strauss, H. W. Development and characterization of annexin V mutants with endogenous chelation sites for (99m)Tc. Bioconj. Chem., *11:* 918–925, 2000.
17. Blankenberg, F., Ohtsuki, K., and Strauss, H. W. Dying a thousand deaths. Radionuclide imaging of apoptosis. Quart. J. Nucl. Med., *43:* 170–176, 1999.
18. Blankenberg, F. G., Katsikis, P. D., Tait, J. F., Davis, R. E., Naumovski, L., Ohtsuki, K., Kopiwoda, S., Abrams, M. J., Darkes, M., Robbins, R. C., Maecker, H. T., and Strauss, H. W. *In vivo* detection and imaging of phosphatidylserine expression during programmed cell death. Proc. Natl. Acad. Sci. USA, *95:* 6349–6354, 1998.
19. Narula, J., Acio, E. R., Narula, N., Samuels, L. E., Fyfe, B., Wood, D., Fitzpatrick, J. M., Raghunath, P. N., Tomaszewski, J. E., Kelly, C., Steinmetz, N., Green, A., Tait, J. F., Leppo, J., Blankenberg, F. G., Jain, D., and Strauss, H. W. Annexin-V imaging for noninvasive detection of cardiac allograft rejection. Nat. Med., *7:* 1347–1352, 2001.

20. Russell, J., O'Donoghue, J. A., Finn, R., Koziorowski, J., Ruan, S., Humm, J. L., and Ling, C. C. Iodination of annexin V for imaging apoptosis. J. Nucl. Med., *43:* 671–677, 2002.
21. Yang, D. J., Azhdarinia, A., Wu, P., Yu, D. F., Tansey, W., Kalimi, S. K., Kim, E. E., and Podoloff, D. A. *In vivo* and *in vitro* measurement of apoptosis in breast cancer cells using 99mTc-EC-annexin V. Cancer Biother. Radiopharm., *16:* 73–83, 2001.
22. Zhao, M., Beauregard, D. A., Loizou, L., Davletov, B., and Brindle, K. M. Non-invasive detection of apoptosis using magnetic resonance imaging and a targeted contrast agent. Nat. Med., *7:* 1241–1244, 2001.
23. Schellenberger, E. A., Bogdanov, A., Jr., Hogemann, D., Tait, J., Weissleder, R., and Josephson, L. Annexin V-CLIO: a nanoparticle for detecting apoptosis by MRI. Mol. Imaging, *1:* 102–107, 2002.
24. Wood, B. L., Gibson, D. F., and Tait, J. F. Increased erythrocyte phosphatidylserine exposure in sickle cell disease: flow-cytometric measurement and clinical associations. Blood, *88:* 1873–1880, 1996.
25. Vermes, I., Haanen, C., Steffens-Nakken, H., and Reutelingsperger, C. A novel assay for apoptosis. Flow cytometric detection of phosphatidylserine expression on early apoptotic cells using fluorescein labelled Annexin V. J. Immunol. Methods, *184:* 39–51, 1995.
26. Dumont, E. A., Reutelingsperger, C. P., Smits, J. F., Daemen, M. J., Doevendans, P. A., Wellens, H. J., and Hofstra, L. Real-time imaging of apoptotic cell-membrane changes at the single-cell level in the beating murine heart. Nat. Med., *7:* 1352–1355, 2001.
27. Hawrysz, D., and Sevick-Muraca, E. Developments toward diagnostic breast cancer imaging using near-infrared optical measurements and fluorescent contrast agents. Neoplasia, *2:* 388–417, 2000.
28. Ntziachristos, V., Bremer, C., Graves, E. E., and Weissleder, R. *In-vivo* tomographic imaging of near-infrared fluorescent probes. Mol. Imaging, *1:* 82–88, 2002.
29. Ntziachristos, V., Tung, C-H., Bremer, C., and Weissleder, R. Fluorescence molecular tomography resolves protease activity *in vivo.* Nat. Med., *8:* 757–760, 2002.
30. Browder, T., Butterfield, C., Kraling, B., Shi, B., Marshall, B., O'Reilly, M., and Folkman, J. Antiangiogenic scheduling of chemotherapy improves efficacy against experimental drug-resistant cancer. Cancer Res., *60:* 1878–1886, 2000.
31. Moore, A., Marecos, E., Simonova, M., Weissleder, R., and Bogdanov, A., Jr. Novel gliosarcoma cell line expressing green fluorescent protein: a model for quantitative assessment of angiogenesis. Microvasc. Res., *56:* 145–153, 1998.
32. Bogdanov, A., Jr., Lin, C., Simonova, M., Matuszewski, L., and Weissleder, R. Cellular activation of the self-quenched fluorescent reporter probe in tumor microenvironment. Neoplasia, *4:* 228–236, 2002.
33. Petrovsky, A. V., Browder, T., Weissleder, R., Mustafa, M., and Bogdanov, A., Jr. MRI monitoring of anti-angiogenic effects in drug-resistant Lewis lung carcinoma. Proceedings of 2002 Keystone Symposia: "Angiogenesis in Cancer and Other Diseases: From Genes to Function to Therapy," Banff, Alberta, Canada, February 8–13, p. 154, 2002.
34. Mahmood, U., Tung, C. H., Bogdanov, A., Jr., and Weissleder. R. Near-infrared optical imaging of protease activity for tumor detection. Radiology, *213:* 866–870, 1999.
35. Blankenberg, F. G., Naumovski, L., Tait, J. F., Post, A. M., and Strauss, H. W. Imaging cyclophosphamide-induced intramedullary apoptosis in rats using 99mTc-radiolabeled annexin V. J. Nucl. Med., *42:* 309–316, 2001.
36. Ogura, Y., Krams, S. M., Martinez, O. M., Kopiwoda, S., Higgins, J. P., Esquivel, C. O., Strauss, H. W., Tait, J. F., and Blankenberg, F. G. Radiolabeled annexin V imaging: diagnosis of allograft rejection in an experimental rodent model of liver transplantation. Radiology, *214:* 795–800, 2000.
37. Vriens, P. W., Blankenberg, F. G., Stoot, J. H., Ohtsuki, K., Berry, G. J., Tait, J. F., Strauss, H. W., and Robbins, R. C. The use of technetium Tc 99m annexin V for *in vivo* imaging of apoptosis during cardiac allograft rejection. J. Thoracic Cardiovasc. Surg., *116:* 844–853, 1998.
38. Schellenberger, E. A., Bogdanov A., Jr., Petrovsky, A., Ntziachristos, N., Weissleder, R., and Josephson, L. Optical imaging of apoptosis as a biomarker of tumor response to chemotherapy. Neoplasia, in press, 2003.
39. Chishima, T., Miyagi, Y., Wang, X., Yamaoka, H., Shimada, H., Moossa, A. R., and Hoffman, R. M. Cancer invasion and micrometastasis visualized in live tissue by green fluorescent protein expression. Cancer Res., *57:* 2042–2047, 1997.
40. Yang, M., Baranov, E., Moossa, A. R., Penman, S., and Hoffman, R. M. Visualizing gene expression by whole-body fluorescence imaging. Proc. Natl. Acad. Sci. USA, *97:* 12278–12282, 2000.
41. Fukumura, D., Xavier, R., Sugiura, T., Chen, Y., Parks, E. C., Lu, N., Selig, M., Nielson, G., Taksir, T., Jain, R. K., and Seed, B. Tumor induction of VEGF promoter activity in stromal cells. Cell, *94:* 715–725, 1998.
42. Boehm, T., Folkman, J., Browder, T., and O'Reilly. M. S. Antiangiogenic therapy of experimental cancer does not induce acquired drug resistance. Nature (Lond.), *390:* 404–407, 1997.
43. Hammill, A. K., Uhr, J. W., and Scheuermann, R. H. Annexin V staining due to loss of membrane asymmetry can be reversible and precede commitment to apoptotic death. Exp. Cell Res., *251:* 16–21, 1999.
44. Ntziachristos, V., Ripoli, J., and Weissleder, R. Would near-infrared fluorescence signals propagate through large human organs for clinical studies? Opt. Lett., *27:* 333–335, 2002.

Near-Infrared Fluorescent Imaging of Tumor Apoptosis

Alexander Petrovsky, Eyk Schellenberger, Lee Josephson, et al.

Cancer Res 2003;63:1936-1942.